Finite Element Modelling of Pressure Loss in an Idealised Stenosed Valve

How does idealised stenotic valve geometry influence flow structure and pressure drop at peak systole, as predicted using finite element modelling?

6CCYB060 Applied Finite Elements

George Welling

Module Lead: Dr Adelaide De Vecchi

School of Biomedical Engineering and Imaging Sciences

King's College London

January 2026

Table of Contents

1 Introduction

Aortic valve stenosis (AVS) is a major valvular heart disease in ageing populations, affecting 3% of people older than 65 years[1], and represents a major cause of morbidity and mortality worldwide. The disease is characterised by progressive calcification and thickening of the aortic valve leaflets, which reduces valve mobility and limits the effective orifice during systole. As a consequence, blood ejected from the left ventricle is forced through a narrowed opening, leading to the formation of a high velocity jet downstream of the valve and a significant pressure drop across it.[1,2] This increased pressure load places excessive mechanical demand on the left ventricle, often resulting in ventricular hypertrophy, heart failure, and reduced cardiac output if left untreated.

Current clinical management of severe aortic valve stenosis includes surgical aortic valve replacement (SAVR); however, a substantial proportion of the affected population are deemed unsuitable[3] for major surgery due to advanced age or comorbidities. As a result, since its introduction, transcatheter aortic valve implantation (TAVI) has been increasingly adopted as an effective alternative, particularly for high-risk patients, with consistently favourable clinical outcomes[2,3]. Assessment of stenosis severity and procedural success is most commonly performed using Doppler echocardiography which estimates transvalvular velocity and pressure gradients across the valve[2]. While non-invasive and widely available, this approach is highly dependent on operator expertise, Doppler angle alignment and acoustic window quality, all of which can affect the accuracy of velocity and pressure gradient estimation in aortic stenosis. Moreover, the simplified assumptions underlying Doppler-based measurements may not fully capture the complex hemodynamics associated with stenotic valve geometries. These limitations highlight the need for physics-based computational approaches capable of resolving the full velocity and pressure fields within stenosed valves.

Computational modelling has emerged as a powerful and widely used tool to complement clinical assessment by providing detailed, physics-based insight and an objective secondary evaluation that is not dependent on operator experience. Among these approaches, the finite element method (FEM) is a numerical technique originally developed to model the mechanical response of structures under applied loads through discretisation of a complex domain into smaller elements. Advances in computational power and medical imaging have enabled FEM to be increasingly applied to patient-specific biomedical problems, including cardiovascular flow modelling[4,7]. In the context of aortic valve stenosis, FEM allows the governing equations of mass and momentum conservation to be solved within realistic geometries enabling a detailed prediction of velocity fields and pressure distributions in cardiovascular flow systems, that cannot be directly measured in vivo[5,8]. As such, FEM provides a robust framework for quantifying pressure loss in stenotic flow configurations and characterising the hemodynamic consequences of stenotic valve flow[9]. Importantly, idealised geometries allow individual geometric and flow parameters to be controlled independently, enabling mechanistic investigation of pressure loss and jet behaviour that is not feasible in clinical studies.

Despite advances in imaging and modelling, knowledge gaps remain. Currently transthoracic Doppler echocardiography remains the cornerstone of aortic stenosis assessment, often using a simplified Bernoulli equation to calculate pressure gradient[6]. However, its accuracy is constrained by several methodological limitations. Measurements of transvalvular velocity and pressure gradients are inherently sensitive to image acquisition and beam orientation and

require precise optimisation of Doppler settings and angle correction[10], making the technique dependent on operator expertise and acoustic window quality. Incomplete alignments between the Doppler beam and the high-velocity jet can result in systematic underestimation of peak velocities, with misalignment reported in approximately 20% of clinical studies[6]. In addition, Doppler-based pressure estimates do not explicitly account for downstream pressure recovery or complex flow features such as jet expansion and recirculation, which can alter the true hemodynamic load imposed on the left ventricle. These effects contribute to the discrepancies between Doppler-derived gradients and invasive measurements and highlight the limitations of relying solely on simplified, one-dimensional flow for assumptions of stenosis severity classification.

This project employs a finite element model to simulate steady blood flow through an idealised stenosed aortic valve geometry at peak systole. Under the assumptions of incompressible, viscous flow and negligible temporal acceleration at peak flow, the conservation of mass and momentum equations are solved to predict velocity and pressure fields throughout the valve domain. The computation of the mean pressure drop between the inlet and outlet boundaries is computed as a numerical analogue of the clinically relevant transvalvular pressure gradient.

Although Doppler echocardiography remains the standard clinical tool for estimating pressure gradients, its reliance on simplified flow assumptions and operator-dependent measurements may obscure the true hemodynamic burden imposed by a stenosed valve. In contrast, physics-based computational modelling enables a systematic investigation of flow-pressure relationships within controlled geometries, providing detailed insights into jet formation and pressure loss mechanisms that are challenging to assess in vivo.

Accordingly, the present study investigates, *how does idealised stenotic valve geometry influence flow structure and pressure drop at peak systole, as predicted using finite element modelling?*

2 Review

To contextualise the present modelling approach, this section reviews a representative finite element study[11] that addresses pressure loss in stenotic cardiovascular flow.

2.1 Computational modelling of pressure loss in stenotic flow

Pressure loss in stenotic cardiovascular flow is of major clinical importance, as it is the foundation of the assessment of disease severity and directly influences treatment decisions. In current clinical practice, transvalvular pressure gradients are most commonly estimated using Doppler echocardiography; however, these measurements are sensitive to operator expertise, Doppler beam alignment and acoustic window quality, introducing additional uncertainty into pressure drop calculations. As a result, accurately quantifying the true hemodynamic situation imposed by a stenosis remains challenging.

Computational modelling offers a physics-based alternative for assessing pressure loss that is independent of operator variability. In particular, the finite element method (FEM) enables numerical solution of the Navier-Stokes equations within specified geometries, providing detailed predictions of velocity and therefore pressure fields throughout the flow domain. Such models can complement clinical measurements by offering a framework for pressure drop estimation and facilitating mechanistic insight into stenotic flow behaviour.

2.2 Finite element formulation and modelling assumptions

The study by Failer et al. (2021), "On the Impact of Fluid Structure Interaction in Blood Flow Simulations", employs finite element solutions of the Navier-Stokes equations to quantify pressure loss and hemodynamic indices in stenotic flow configurations, thereby directly addressing limitations associated with simplified clinical measurement techniques.

The flow of an incompressible fluid can be described by the Navier-Stokes equations, which enforce conservation of momentum and mass for a fluid of constant density and viscosity. In the study by Failer et al. (2021), blood is modelled as an incompressible Newtonian fluid, and the governing equations are written as

$$\rho_f\left(\partial_t \boldsymbol{v}_f + \left(\boldsymbol{v}_f \bullet \nabla\right)\boldsymbol{v}_f\right) - \mu_f \, div\left(\nabla \boldsymbol{v}_f + \nabla \boldsymbol{v}_f^T\right) + \nabla p_f = 0 \quad in\ \mathcal{F}, \tag{1a}$$

$$div\ \boldsymbol{v}_f = 0 \quad in\ \mathcal{F}. \tag{1b}$$

Here, $\boldsymbol{v}_f$ denotes the fluid velocity field, p_f the pressure, ρ_f the fluid density and μ_f the dynamic viscosity. These equations form the basis of the finite element formulation used to compute velocity and pressure fields within the stenotic domain.

Failer et al. employ the finite element method to solve the incompressible Navier-Stokes equations (1a-1b) within a stenotic flow domain. The computational domain is discretised into unstructured finite elements, allowing complex stenotic geometries to be represented accurately while maintaining numerical stability. A weak formulation of the governing equations is constructed, enabling the coupled velocity-pressure fields to be solved using appropriate finite element to ensure stable and physically consistent solutions for the coupled velocity-pressure fields. This FEM framework allows spatially resolved predictions of velocity and pressure, from which pressure loss is directly computed.

In contrast to simplified analytical approaches, the finite element formulation captures nonlinear effects within the stenosis. Although the study incorporates fluid-structure interaction (FSI) to account for vessel wall motion, the underlying FEM treatment of the fluid domain remains directly relevant to rigid-wall stenotic flow simulations. In the present project, a similar finite element solution of the Navier-Stokes equations is adopted, but with the simplifying assumption of a fixed geometry and steady flow at peak systole, enabling focused investigation of pressure loss mechanisms while reducing computational complexity.

Failer et al. considered an idealised three-dimensional coronary artery geometry composed of straight inflow and outflow sections connected by a curved segment. Stenosis was introduced either symmetrically or asymmetrically along the inner curvature of the vessel, enabling systematic investigation of how curvature and geometric asymmetry influences pressure loss and flow patterns. This controlled setup allowed the effects of wall compliance and stenotic geometry to be isolated without the variability of patient-specific anatomy.

2.3 Key findings and relevance to the present study

Rigid-wall Navier-Stokes simulations are compared with fully coupled fluid-structure interaction models in idealised stenotic coronary artery geometries. A principal result concerns pressure loss and computational fractional flow reserve (cFFR) across the stenosis. In the FSI simulations, stenotic cases exhibited a reduction in pressure of approximately 5%,

indicating a moderate but physiologically relevant functional impairment. By contrast, the rigid-wall Navier-Stokes model showed a similar magnitude of pressure change, ~5%, which authors suggest is influenced strongly by vessel curvature in addition to the stenosis geometry.

Analysis of pressure amplitude further highlighted difference between modelling approaches. In rigid-wall simulations, the pressure oscillation amplitude downstream of the stenosis decreased by approximately 7.5%, with little distinction between healthy and stenotic geometries. In comparison, the FSI simulations showed a smaller reduction around 5%, reflecting the damping effect of vessel wall compliance under loading.

Despite these differences, the rigid-wall simulations were shown to capture the dominant hemodynamic behaviour, including flow acceleration through the stenosis and the overall pressure drop across the narrowed region. The influence of FSI primarily introduced secondary corrections to pressure magnitude rather than altering the quantitative flow response. This suggests that rigid-wall finite element models remain appropriate for studies primarily focused on stenosis-induced pressure loss.

The study employs idealised three-dimensional geometries, which enables systematic comparison between modelling approaches but limits direct applicability to patient-specific anatomy. Blood is modelled as an incompressible Newtonian fluid, an assumption that is generally acceptable for large arteries but neglects non-Newtonian effects that may arise in highly disturbed flow regions.

While the FSI formulation incorporates minor vessel wall motion, the arterial wall is represented as a homogeneous material, not taking into consideration layered structure. Additionally, the fully coupled ALE FSI framework is computationally expensive, which may restrict its use in large parametric studies or simplified modelling pipelines.

Overall, the results indicate that although FSI improves physical realism, rigid-wall finite element simulations provide a computationally efficient and defensible approximation for pressure-focused analyses, particularly when wall deformation is expected to be small or secondary to the primary flow features.

The findings of Failer et al. therefore support the use of rigid-wall finite element models as a computationally efficient and physiological meaningful approach for investigating pressure loss in stenotic cardiovascular flows, particularly when the primary objective is comparative or mechanistic analysis rather than absolute clinical prediction.

3 Methodology

This study employs a finite element modelling approach to investigate pressure loss associated with flow through an idealised stenosed valve under peak systolic conditions. Blood is modelled as an incompressible, viscous fluid governed by Navier-Stokes equations, with flow assumed to be fully developed at peak systole such that temporal acceleration effects are negligible. A rigid-wall assumption is adopted to reduce computational complexity and allow focused investigation of stenosis induced flow behaviour[12].

3.1 Computational domain and boundary conditions

The computational domain consists of an idealised two-dimensional stenotic geometry discretised using an unstructured triangular finite element mesh. The mesh and associated boundary segments are shown in Figure 1, where the domain boundaries are partitioned into

four regions, denoted $\Gamma_1, \Gamma_2, \Gamma_3$ and Γ_4, corresponding to the imposed boundary conditions. The inlet boundary, Γ_1, is located on the right-hand side of the domain and prescribes the inflow velocity. The outlet boundary, Γ_2, is located on the left-hand side of the domain and is treated as a natural outflow boundary. Two additional side outlet boundaries denoted Γ_3, allow flow to exit the domain laterally, acting as the coronary arteries. The remaining boundaries, Γ_4, represent rigid vessel walls on which a no-slip velocity condition is imposed. This boundary configuration enables controlled investigation of pressure loss induced by the stenosis under prescribed inflow conditions.

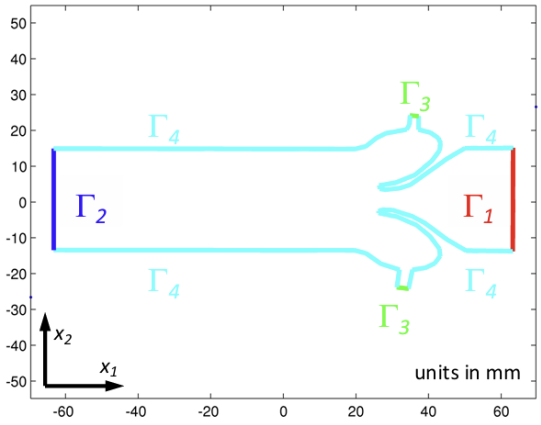

Figure 1: Idealised Stenosed Valve Boundary Geometry

The finite element formulation resolves the coupled velocity and pressure fields throughout the valve domain by solving the governing equations iteratively to convergence. Velocity boundary conditions are prescribed at the inlet and outlets, while pressure emerges naturally from the solution of the flow equations. The resulting pressure field is subsequently used to compute the mean pressure drop between inlet and outlet regions, providing a numerical analogue of the clinically relevant transvalvular pressure gradient[13,15]. This physics-based modelling framework enables systematic investigation of the relationship between stenotic valve geometry, flow structure and pressure loss, independent of operator-dependent clinical measurement techniques.

3.2 Governing equations

Under the assumptions described above, the motion of the fluid is governed by the incompressible Navier-Stokes equations, which enforce conservation of momentum and mass within the flow domain[15],

$$\rho \boldsymbol{v} \bullet \nabla \boldsymbol{v} - \mu \Delta \boldsymbol{v} + \nabla p = 0, \quad on\ \Omega,$$
$$\nabla \bullet \boldsymbol{v} = 0\,, \quad on\ \Omega,$$

where ρ is the fluid density, $\boldsymbol{v}$ is the fluid velocity vector field, μ is dynamic viscosity and p is fluid pressure.

The governing equations are supplemented with appropriate boundary and initial conditions[15]. These conditions represent the imposed inflow and outflow behaviour, and the assumed flow state at the start of the numerical solution. Together, they ensure a well-posed problem and reflect the physical constraints of blood flow through an idealised stenosed valve geometry.

$$\boldsymbol{v} = \boldsymbol{v}_0, \quad on\ \Gamma_1,$$

$$(\mu\nabla \boldsymbol{v} - p\boldsymbol{I}) \bullet \boldsymbol{n} = 0, \ \ \Gamma_2,$$
$$\boldsymbol{v} = \boldsymbol{v}_1, \ \ on\, \Gamma_3,$$
$$\boldsymbol{v} = 0, \ \ on\, \Gamma_4.$$

Where $\boldsymbol{v}$ and p are the flow velocity and pressure, $\rho = 1 \times 10^{-3}\ g\ mm^{-3}$ and $\mu = 4 \times 10^{-2}\ g\ (mm\ s)^{-1}$ are the density and viscosity of the fluid and $\boldsymbol{v}_0, \boldsymbol{v}_1$ are the given boundary data

$$\boldsymbol{v}_0 = (-200, 0)^T mm\ s^{-1}$$

$$\boldsymbol{v}_1 = \begin{cases} (0, 10)^T mm\ s^{-1}, & x_2 > 0 \\ (0, -10)^T mm\ s^{-1}, & x_2 < 0 \end{cases}$$

3.3 Weak formulation

For finite element discretisation, the governing equations are reformulated in weak form by multiplying by test functions and integrating over the fluid domain[14,15]. This formulation forms the basis for constructing the discrete finite element system.

Let $\boldsymbol{w}$ denote a vector test function for velocity and q a scalar test function for pressure. The weak form is derived by multiplying the momentum and continuity equations by test functions

$$(\rho \boldsymbol{v} \bullet \nabla \boldsymbol{v} - \mu\Delta \boldsymbol{v} + \nabla p) \bullet \boldsymbol{w} = 0,$$
$$(\nabla \bullet \boldsymbol{v}) \bullet q = 0,$$

and then integrating over the fluid domain Ω yields,

$$\int (\rho \boldsymbol{v} \bullet \nabla \boldsymbol{v} - \mu\Delta \boldsymbol{v} + \nabla p) \bullet \boldsymbol{w}\, d\Omega = 0\,,$$
$$\int (\nabla \bullet \boldsymbol{v}) \bullet q\, d\Omega = 0,$$

Integration by parts is then applied to the viscosity and pressure terms to naturally incorporate boundary conditions.

$$\int \big((\rho \boldsymbol{v} \bullet \nabla \boldsymbol{v}) \bullet \boldsymbol{w} - (\mu\Delta \boldsymbol{v}) \bullet \boldsymbol{w} + (\nabla p) \bullet \boldsymbol{w}\big)\, d\Omega = 0,$$
$$\int (\rho \boldsymbol{v} \bullet \nabla \boldsymbol{v}) \bullet \boldsymbol{w}\, d\Omega - \int (\mu\Delta \boldsymbol{v}) \bullet \boldsymbol{w}\, d\Omega + \int \nabla p \bullet \boldsymbol{w}\, d\Omega = 0,$$
$$\int \rho(\boldsymbol{v} \bullet \nabla)\boldsymbol{v} \bullet \boldsymbol{w}\, d\Omega + \int \mu\nabla \boldsymbol{v} : \nabla \boldsymbol{w}\, d\Omega - \int p\nabla \bullet \boldsymbol{w}\, d\Omega = \int \mu(\nabla \boldsymbol{v} \bullet \boldsymbol{n}) \bullet \boldsymbol{w}\, d\Gamma - \int (p\boldsymbol{w}) \bullet \boldsymbol{n}\, d\Gamma.$$

The boundary integral vanishes for velocity/pressure (Dirichlet) boundaries, leaving the final weak form:

$$\int \rho(\boldsymbol{v} \bullet \nabla)\boldsymbol{v} \bullet \boldsymbol{w}\, d\Omega + \int \mu\nabla \boldsymbol{v} : \nabla \boldsymbol{w}\, d\Omega - \int p\nabla \bullet \boldsymbol{w}\, d\Omega = 0,$$
$$\int q\nabla \bullet \boldsymbol{v}\, d\Omega = 0.$$

3.4 Finite element discretisation

The weak form of the incompressible Navier-Stokes equations is discretised in space using the finite element method. The computational domain is partitioned into a mesh of triangular elements, allowing the stenosed valve geometry to be represented accurately[15].

The velocity and pressure fields are approximated using separate finite element spaces with different polynomial orders. The velocity field is interpolated using quadratic basis functions, while the pressure field is interpolated using linear basis functions. This mixed-order interpolation enables stable numerical approximation of the coupled velocity-pressure system in incompressible flow simulations.

Within each element, the velocity and pressure are expressed as linear contributions of their respective basis functions and nodal coefficients. Substitution of these discrete approximations into the weak formulation yields a coupled system of nonlinear equations. Numerical integration of the element-level contributions is performed using Gaussian quadrature, with a sufficiently high quadrature order to accurately evaluate the nonlinear terms.

3.5 Nonlinear solution procedure

The incompressible Navier-Stokes equations are nonlinear due to the presence of velocity-dependent term. As a result, the finite element discretisation yields a coupled system of nonlinear equations for the velocity and pressure degrees of freedom. To solve this system, an iterative Newton-Raphson procedure is employed.

At each iteration, the residual vector corresponding to the discretised momentum and continuity equations is assembled based on the current estimates of the velocity and pressure fields. The Jacobian matrix, representing the linearisation of the residual with respect to the unknowns, is constructed numerically. The resulting linear system is then solved to obtain an update to the velocity and pressure fields.

Iterations are repeated until convergence is achieved, which is assessed using the Euclidean norm of the global residual vector. The solution is considered converged when this norm falls below a predefined tolerance of 10^{-6}.

3.6 Pressure drop post-processing

Following convergence of the finite element solution, the pressure field is available throughout the computational domain as part of the coupled velocity-pressure solution. To quantify the hemodynamic impact of the stenosis, the pressure drop across the valve is computed as a post processing step.

The transvalvular pressure drop is defined as the difference between the spatially averaged pressure at a prescribed upstream inlet region and a downstream outlet region. Specifically, mean pressures are evaluated over the inlet and outlet boundaries to reduce sensitivity to local numerical fluctuations and to provide a representative measure of the global pressure loss induced by the stenosis. The pressure drop is then calculated as:

$$\Delta p = \bar{p}_{inlet} - \bar{p}_{outlet}.$$

This definition is consistent with clinically relevant pressure gradients used to assess stenosis severity, while allowing direct computation from the numerical solution without reliance on simplified analytical assumptions. By evaluating pressure loss directly from the resolved pressure field, the finite element model enables a physically consistent assessment of flow resistance associated with the stenotic geometry.

The finite element formulation yields converged velocity and pressure fields throughout the stenotic valve domain. These outputs are used to quantify flow acceleration, jet structure and the mean pressure drop between inlet and outlet regions, providing a numerical analogue of the transvalvular pressure gradient. The following section presents and analyses these results in relation to stenotic geometry under peak systolic conditions.

4 Results

The results in this section summarise the velocity and pressure fields obtained from the finite element simulations of flow through an idealised stenosed valve geometry. To illustrate the characteristic hemodynamic behaviour, velocity and pressure distributions obtained using the finest mesh resolution are first presented. This mesh was selected to ensure adequate spatial resolution of the high-velocity jet and steep pressure gradients that develop across the stenosis. The figures that follow highlight the acceleration of flow through the narrowed region and the associated pressure drop across the domain, which together underpin the quantitative pressure loss analysis presented later in this section.

In this study, four increasingly refined finite element meshes are used to evaluate the pressure drop across the idealised stenosed valve geometry. The use of multiple mesh resolutions allows assessment of the sensitivity of the computed pressure drop to spatial discretisation and provides a convergence check under increasing computational resolution. Figures showing velocity field and pressure map are from the highest level of refinement.

4.1 Mesh refinement and convergence analysis

Table 1 summarises the mesh refinement levels, quantified by the total number of nodes, together with the corresponding transvalvular pressure drop calculated between the inlet (Γ_1) and outlet (Γ_2) boundaries.

Mesh Refinement Level	Number of Velocity Nodes	Pressure Drop (mmHg)
0	1,842	7.3870
1	3,029	8.6436
2	7,968	8.4023
3	16,017	8.6707

Table 1: Mesh refinement level, total number of nodes and computed transvalvular pressure drop between inlet (Γ_1) and outlet (Γ_2) boundaries.

Mesh refinement analysis was performed to assess numerical convergence of the computed pressure drop and to ensure that results were independent of mesh resolution, shown in Figure 2.

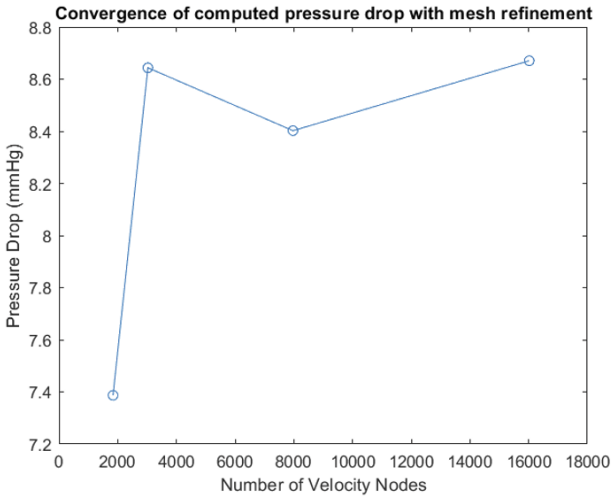

Figure 2: Mesh convergence of transvalvular pressure drop

4.2 Velocity field

Flow through the idealised stenosed valve is visualised using a velocity vector field, as shown in Figure 3. As the flow enters the stenotic region, the reduction in cross-sectional area leads

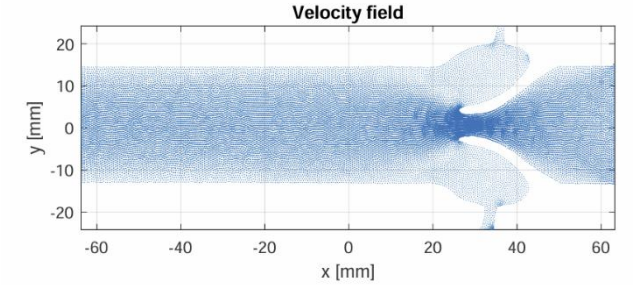

Figure 3: Velocity Vector Map (mm s^{-1}) of Idealised Stenosed Valve

to an increase in the acceleration of the fluid, resulting in the formation of a high-velocity jet downstream of the narrowing. This behaviour is consistent with conservation of mass and is characteristic of flow through stenotic geometries.

4.3 Pressure field and pressure loss

Flow acceleration through the stenotic region produces a pronounced high-velocity jet, as shown in Figure 3, with velocity magnitude increasing sharply as the flow passes through the narrowed valve orifice. This acceleration is accompanied by a significant pressure decrease across the constriction, clearly visible in the pressure distribution shown in Figure 4. The formation of large pressure gradients across the stenosis is consistent with the momentum balance in the incompressible Navier-Stokes equations, specifically the momentum equation,

$$\rho(\boldsymbol{v} \bullet \nabla)\boldsymbol{v} = -\nabla p + \mu\nabla^2\boldsymbol{v},$$

where rapid spatial acceleration of the flow must be balanced by a strong adverse pressure gradient. As velocity increases sharply at the stenosis, pressure drops substantially downstream of the stenosis, flow deceleration and jet expansion leads to partial pressure recovery, as observed in Figure 4.

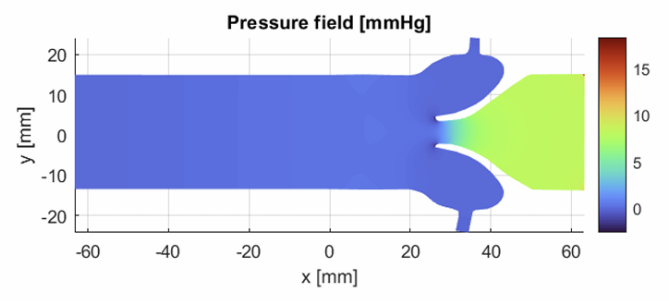

Figure 4: Pressure Map of Idealised Stenosed Valve

The transvalvular pressure drop predicted by the finite element model lies in the range 7.39-8.67 mmHg across the four mesh refinement levels considered. The coarsest mesh yields the lowest pressure drop, indicating under-resolution of the high velocity gradients within the stenotic region. As the mesh is refined, the predicted pressure drop increases and stabilises, reflecting improved numerical representation of the accelerated jet formed through the stenosis and the associated pressure loss mechanisms. The converged pressure drop is of order 8.5-8.7 mmHg, which is physiologically reasonable for an idealised stenosis configuration under peak systolic flow conditions. These results demonstrate that the finite element model is capable of capturing the dominant hemodynamic features governing pressure loss in stenotic valve flow.

4.4 Error analysis and convergence assessment

A mesh convergence study was performed to assess the numerical stability and accuracy of the finite element solution. The pressure drop was evaluated for four increasingly refined meshes, and its variation with refinement was examined as a measure of convergence of the numerical scheme. A significant change of approximately 14.5% was observed between the coarsest and most refined mesh, indicating that the initial discretisation was insufficient to resolve the flow features within the stenosis, in contrast the pressure drop predictions on the two finest meshes differed by approximately 3%, suggesting that the solution is approaching mesh independence. This reduction in sensitivity to further mesh refinement indicates that discretisation error is small at higher resolutions.

Convergence was identified through the reduction of the residual norm, implementing the Newton-Raphson method and defined as the reduction of the Euclidean norm of the global residual vector below 10^{-6}. Table 2 shows the norm of the residual vector after each iteration for each level of mesh refinement, which demonstrates the stability of the solver.

	Residual Norm Calculations				
Mesh Level Refinement	**Iteration 0**	**Iteration 1**	**Iteration 2**	**Iteration 3**	**Iteration 4**
0	26.5189	1.8663	0.082985	5.364×10^{-5}	2.3885×10^{-10}
1	41.2765	2.1166	0.10306	9.2693×10^{-5}	5.2051×10^{-10}
2	56.6017	1.6974	0.066498	4.8913×10^{-5}	4.1120×10^{-10}
3	80.025	1.3102	0.051427	3.7258×10^{-5}	4.5760×10^{-10}

Table 2: Summary of Newton-Raphson convergence behaviour for all mesh level refinements.

The finite element simulations successfully resolved the velocity and pressure fields associated with flow through an idealised stenosed valve at peak systole. Flow acceleration through the constriction produced a high-velocity jet and a corresponding pressure drop across the stenosis. Mesh refinement demonstrated convergence of the predicted pressure drop, with only small changes observed at higher resolutions.

5 Discussion

5.1 Interpretation of results

The following discussion considers the physiological relevance of these findings, the influence of modelling assumptions and the limitations of the present approach.

The results demonstrate flow behaviour consistent with fundamental principles of fluid mechanics and known hemodynamics of stenotic valves. As flow passes through the narrowed valve region, conservation of mass requires an increase in velocity, resulting in the formation of a high-velocity jet downstream of the stenosis. This acceleration is accompanied by a reduction in static pressure across the constriction, reflecting the increased kinetic energy within the flow. Downstream of the stenosis, partial pressure recovery is observed as the jet expands and decelerates. These features are characteristic of stenotic cardiovascular flow and support the physical validity of the numerical solution.

The predicted transvalvular pressure drop of approximately 7-9 mmHg lies within a physiologically reasonable range for an idealised stenosis under peak systolic conditions[16]. While the present model does not aim to reproduce patient-specific disease severity, the magnitude of the pressure drop reflects a moderate flow obstruction and is consistent with expectations for simplified stenotic geometries. Importantly, the pressure drop is computed directly from the resolved pressure field rather than inferred from velocity measurements, highlighting the advantage of physics-based modelling for mechanistic assessment of flow resistance.

The mesh refinement study demonstrated convergence of the predicted pressure drop, with diminishing changes observed as mesh resolution increased. Beyond the intermediate refinement levels, further increases in node count produced only minor variations in pressure drop, indicating that the solution is effectively mesh-independent. This behaviour confirms that the numerical scheme and discretisation are sufficiently resolved to capture the dominant flow and pressure features of the problem, providing confidence in the reported results.

5.2 Model limitations

A primary limitation of the present model is the rigid-wall assumption, which neglects deformation of the vessel or valve structure in response to flow-induced loads[11]. In physiological conditions, wall compliance can damp pressure fluctuations and slightly reduce peak pressure gradients. As a result, rigid-wall simulations may overestimate pressure loss compared to fully coupled fluid-structure interaction models. Previous studies have shown that rigid-wall formulations capture the dominant hemodynamic behaviour in stenotic flows, particularly when the primary interest is relative pressure loss rather than absolute clinical prediction. In this context, the rigid-wall assumption represents a reasonable trade-off between physical fidelity and computation efficiency.

Additional simplifying assumptions include the use of steady-state flow at peak systole and modelling blood as an incompressible Newtonian fluid. While real cardiovascular flow is pulsatile and blood exhibits non-Newtonian behaviour at low shear rates, these effects are

expected to play a secondary role in the high-shear, peak-flow conditions considered here[11]. The use of an idealised stenosed geometry further limits direct applicability to patient-specific cases; however, it enables controlled investigation of fundamental flow-pressure relationships without confounding anatomical variability.

In summary, the finite element model successfully quantified pressure loss associated with flow through an idealised stenosed valve and demonstrated robust numerical convergence. Despite its simplifying assumptions, the model captures key hemodynamic features of stenotic flow and provides a solid foundation for more advanced, physiologically detailed simulations.

6 References

(1) Grimard BH, Safford RE, Burns EL. Aortic Stenosis: Diagnosis and Treatment. Am Fam Physician. 2016 Mar 1;93(5):371-8. PMID: 26926974.

(2) Wiegerinck EM, van de Hoef TP, Rolandi MC, Yong Z, van Kesteren F, Koch KT, Vis MM, de Mol BA, Piek JJ, Baan J Jr. Impact of Aortic Valve Stenosis on Coronary Hemodynamics and the Instantaneous Effect of Transcatheter Aortic Valve Implantation. Circ Cardiovasc Interv. 2015 Aug;8(8):e002443. doi: 10.1161/CIRCINTERVENTIONS.114.002443. PMID: 26245891.

(3) Howard C, Jullian L, Joshi M, Noshirwani A, Bashir M, Harky A. TAVI and the future of aortic valve replacement. J Card Surg. 2019 Dec;34(12):1577-1590. doi: 10.1111/jocs.14226. Epub 2019 Oct 10. PMID: 31600005.

(4) Ghouchani A, Ebrahimzadeh MH. Can Patient-specific Finite Element Models Enter Clinical Practice as a Decision Support System? Arch Bone Jt Surg. 2021 Jan;9(1):1-4. doi: 10.22038/abjs.2020.54579.2722. PMID: 33778109; PMCID: PMC7957102.

(5) Nada A, Fakhr MA, El-Wakad MTI, Hassan MA. A Finite Element-Based Analysis of a Hemodynamics Efficient Flow Stent Suitable for Different Abdominal Aneurysm Shapes. J Biomech Eng. 2022 Sep 1;144(9):091006. doi: 10.1115/1.4053999. PMID: 35237800.

(6) Karelas D, Tatsis E, Oikonomidis D, Papadopoulos CH. Diagnostic Challenges in the Management of Aortic Valfvelocityve Stenosis and the Role of Imaging: A Narrative Review. *Journal of Clinical Medicine*. 2025; 14(4):1231. https://doi.org/10.3390/jcm14041231

(7) Liu, W.K., Li, S. & Park, H.S. Eighty Years of the Finite Element Method: Birth, Evolution, and Future. *Arch Computat Methods Eng* **29**, 4431–4453 (2022). https://doi.org/10.1007/s11831-022-09740-9

(8) Spühler JH, Jansson J, Jansson N, Hoffman J. 3D fluid-structure interaction simulation of aortic valves using a unified continuum ALE FEM model. *Front Physiol*. 2018 Apr 16;9:363. doi:10.3389/fphys.2018.00363

(9) Lyras KG, LEE J. Comparison of numerical implementations for modelling flow through arterial stenoses. *Int J Mech Sci*. 2021;198:106780. doi:10.1016/j.ijmecsci.2021.1068780

(10) Manzo R, Ilardi F, Nappa D, Mariani A, Angellotti D, Immobile Molaro M, Sgherzi G, Castiello DS, Simonetti F, Santoro C, Canonico ME, Avvedimento M, Piccolo R, Franzone A, Esposito G. Echocardiographic Evaluation of Aortic Stenosis: A Comprehensive Review. Diagnostics (Basel). 2023 Jul 29;13(15):2527. doi: 10.3390/diagnostics13152527. PMID: 37568890; PMCID: PMC10417789.
(11) Failer L, Minakowski P, Richter T. On the impact of fluid structure interaction in blood flow simulations: stenotic coronary artery benchmark. *Vietnam J Math*. 2021;49(1):169–187. doi:10.1007/s10013-020-00456-6
(12) Jodko D, Jeckowski M, Tyfa Z. Fluid structure interaction versus rigid-wall approach in the study of the symptomatic stenosed carotid artery: Importance of wall compliance and resilience of loose connective tissue. Int J Numer Method Biomed Eng. 2022 Aug;38(8):e3630. doi: 10.1002/cnm.3630. Epub 2022 Jul 10. PMID: 35593678; PMCID: PMC9542585.
(13) Franke B, Weese J, Waechter-Stehle I, Brüning J, Kuehne T, Goubergrits L. Towards improving the accuracy of aortic transvalvular pressure gradients: rethinking Bernoulli. Med Biol Eng Comput. 2020 Aug;58(8):1667-1679. doi: 10.1007/s11517-020-02186-w. Epub 2020 May 26. PMID: 32451697; PMCID: PMC7340661.

(14) Zhang Z, Lee JH, Sun L, Gu GX. Weak-formulated physics-informed modeling and optimization for heterogeneous digital materials. PNAS Nexus. 2024 May 8;3(5):pgae186. doi: 10.1093/pnasnexus/pgae186. PMID: 38818237; PMCID: PMC11137755.
(15) Segal A. Finite element methods for the incompressible Navier–Stokes equations. *Delft University of Technology Lecture Notes*. n.d.
(16) Eerdekens R, Govindarajan V, Johnson NP, Demandt JPA, El Farissi M, Vervaat FE, Johnson DT, Kirkeeide RL, Tonino PAL. Haemodynamic response of normal aortic valves to stress using invasive, non-invasive, and computational techniques. Eur Heart J Imaging Methods Pract. 2025 May 16;3(1):qyaf061. doi: 10.1093/ehjimp/qyaf061. PMID: 40458623; PMCID: PMC12127842.